

Pillar[6]arene/Paraquat Molecular Recognition in Water: High Binding Strength, pH-Responsiveness, and Application in Controllable Self-Assembly, Controlled Release, and Treatment of Paraquat Poisoning

Guocan Yu,[†] Xiangyan Zhou,[‡] Zibin Zhang,[†] Chengyou Han,[†] Zhengwei Mao,[‡] Changyou Gao,[‡] and Feihe Huang^{*†}

[†]MOE Key Laboratory of Macromolecular Synthesis and Functionalization, Department of Chemistry, Zhejiang University, Hangzhou 310027, P. R. China

[‡]MOE Key Laboratory of Macromolecular Synthesis and Functionalization, Department of Polymer Science and Engineering, Zhejiang University, Hangzhou 310027, P. R. China

S Supporting Information

ABSTRACT: The complexation between a water-soluble pillar[6]arene (WP6) and paraquat (G1) in water was investigated. They could form a stable 1:1 [2]pseudorotaxane with an extremely high association constant of $(1.02 \pm 0.10) \times 10^8 \text{ M}^{-1}$ mainly driven by electrostatic interactions, hydrophobic interactions, and π - π stacking interactions. This molecular recognition has not only high binding strength but also pH-responsiveness. The threading and dethreading processes of this [2]pseudorotaxane could be reversibly controlled by changing the solution pH. This novel recognition motif was further used to control the aggregation of a complex between WP6 and an amphiphilic paraquat derivative (G2) in water. The reversible transformations between micelles based on G2 and vesicles based on WP6⊃G2 were realized by adjusting the solution pH due to the pH-responsiveness of WP6. The controlled release of water-soluble dye molecules from the vesicles could be achieved by the collapse of the vesicles into the micelles upon changing the solution pH to acidity. Additionally, the high binding affinity between WP6 and paraquat could be utilized to efficiently reduce the toxicity of paraquat. After the formation of a stable host-guest complex between WP6 and paraquat, less opportunity was available for paraquat to interact with the reducing agents in the cell, which made the generation of its radical cation more difficult, resulting in the efficient reduction of paraquat toxicity.



1. INTRODUCTION

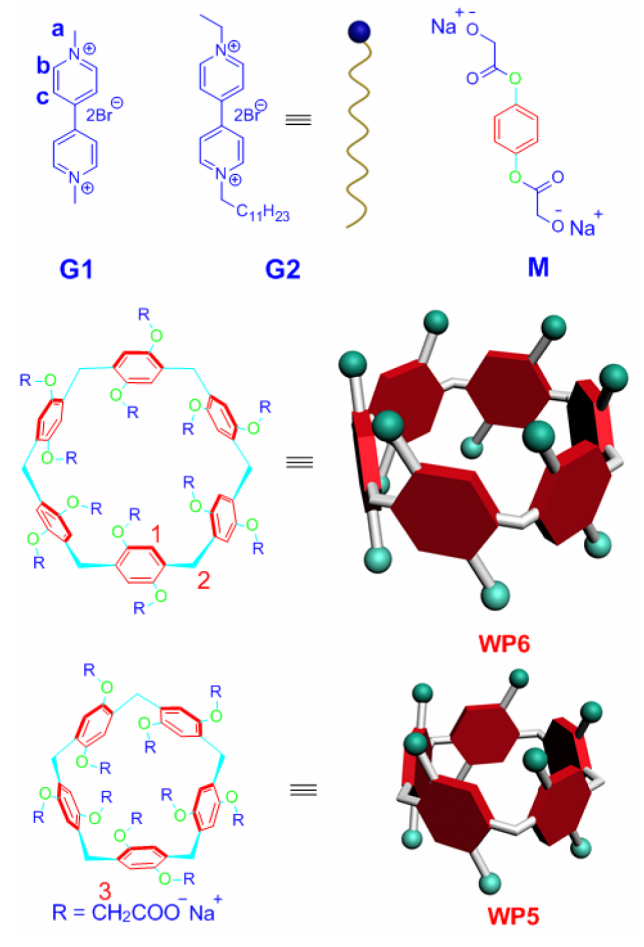
Supramolecular chemistry is being widely studied with the aim of developing sophisticated self-assembly systems, such as molecular machines, supramolecular polymers, supramolecular gels, and other functional supramolecular systems from various building blocks by molecular recognition, self-replication, and self-organization based on noncovalent interactions.¹ Crown ethers,² cyclodextrins,³ calixarenes,⁴ and cucurbiturils⁵ are the four most important classes of macrocyclic hosts and have been widely studied in supramolecular chemistry. Paraquat and its derivatives (*N,N'*-dialkyl-4,4'-bipyridinium salts) have been widely used as guests in supramolecular chemistry to construct numerous host-guest complexes with different macrocyclic hosts.⁶ In order to prepare large supramolecular systems efficiently from small building blocks, we are interested in improving the complexation of paraquat by designing optimized hosts. With the current emphasis on “environment-friendly chemistry”, the search for novel water-soluble hosts with high binding affinities to paraquat and its derivatives is remarkably important.

Pillararenes,^{7–9} mainly including pillar[5]arenes and pillar[6]arenes, are a new type of macrocyclic hosts. Their repeating units are connected by methylene bridges at the *para*-positions, forming a unique rigid pillar architecture, which is different from the basket-shaped structure of *meta*-bridged calixarenes. The unique structure and easy functionalization of pillararenes have afforded them outstanding abilities to selectively bind different kinds of guests and provided a useful platform for the construction of various interesting supramolecular systems, including cyclic dimers,^{7c} chemosensors,⁷ⁱ supramolecular polymers,^{7f} and transmembrane channels.^{7p} The host-guest chemistry of pillar[5]arenes has been widely explored. However, the complexation properties of pillar[6]arenes have been rarely investigated. Herein, we report a novel molecular recognition between a water-soluble pillar[6]arene (WP6, Chart 1) and paraquat (G1, Chart 1). This new recognition motif in water has not only high binding strength but also pH-responsiveness. Furthermore, we utilized this

Received: October 9, 2012

Published: November 6, 2012

Chart 1. Chemicals Used in This Study



recognition motif in controllable self-assembly between **WP6** and an amphiphilic guest (**G2**, Chart 1) containing a hydrophilic 4,4'-bipyridinium unit. Due to the pH-responsiveness of **WP6**,^{8g} the reversible transformations between micelles formed by **G2** alone and vesicles based on **WP6** could be achieved by adjusting the solution pH. These pH-responsive aggregation behaviors were further used in the controlled release of water-soluble dye calcein molecules. Furthermore, the high binding affinity between **WP6** and paraquat was employed to efficiently reduce the toxicity of paraquat.

2. EXPERIMENTAL SECTION

Critical Aggregation Concentration (CAC) Determination of G2 and WP6. Some parameters such as the conductivity, osmotic pressure, fluorescence intensity, and surface tension of the solution change sharply around the critical aggregation concentration. The dependence of the solution conductivity on the solution concentration can be used to determine the critical aggregation concentration. Typically, the slope of the change in the conductivity versus the concentration above the CAC value is smaller than the slope below the CAC value due to the formation of aggregates. Therefore, the junction of the conductivity–concentration plot represents the CAC value. To measure the CAC values of **G2** in the absence and presence of **WP6**, the conductivities of the solutions at different concentrations were determined. By plotting the changes of the conductivity versus the concentration, we could get the CAC values of **G2** and **WP6**.

Transmission Electron Microscopy (TEM) and Dynamic Light Scattering (DLS) Studies. The pH-responsive self-assembled structures of **WP6** were revealed using TEM. A solution of

WP6 (5.00×10^{-4} M) and **G2** (1.00×10^{-3} M) was made first in water. The samples were prepared by drop-coating this solution on a carbon-coated copper grid. TEM experiments were performed on a JEM-1200EX instrument. The solution of **WP6** (5.00×10^{-4} M) and **G2** (1.00×10^{-3} M) was left to stand overnight before being used for DLS tests. Under acidic condition, the precipitate formed by **WP6** was eliminated by using a microporous membrane. The diameters of the assemblies were measured on a Nano-ZS ZEN3600 instrument.

Controlled Release Studies. Calcein (1.25 mg), **WP6** (65.2 mg), and **G2** (40.8 mg) were dissolved in distilled water (20 mL) and under sonication for 30 min. After the sonication, the solution was dialyzed against H_2O for 2 days to remove excess free calcein from water. The dye molecule delivery from the vesicles to the aqueous solution was monitored by the fluorescence intensity at 520 nm ($\lambda_{\text{ex}} = 470$ nm).

Electrochemical Experiments. The cyclic voltammetric measurements were carried out on a CHI600B electrochemical analyzer (Shanghai Chen Hua instruments Co., Ltd.). All the samples were prepared in aqueous solutions at 25 °C, and deoxygenated by purging with dry nitrogen before each experiment. The glassy carbon working electrode was polished with 0.05 μm BAS alumina suspension on a brown Texmet polishing pad, and then washed with ethanol and distilled water before use. The measured potentials were recorded with respect to a Ag/AgCl (immersed in a solution containing saturated potassium chloride) reference electrode. Both of the concentrations of **WP6** and **G1** were 2.00×10^{-4} M. The scan rate is 10 mV/s.

Cell Culture. Raw 264.7 cells, a kind of mouse macrophage cells, were cultured in Dulbecco's modified Eagle's medium (DMEM) containing 10% fetal bovine serum (FBS) and 1% penicillin/streptomycin. Cells grew as a monolayer and were detached upon confluence using trypsin (0.5% w/v in PBS). The cells were harvested from cell culture medium by incubating in trypsin solution for 5 min. The cells were centrifuged, and the supernatant was discarded. A 3 mL portion of serum-supplemented DMEM was added to neutralize any residual trypsin. The cells were resuspended in serum-supplemented DMEM at a concentration of 1×10^4 cells/mL. Cells were cultured at 37 °C and 5% CO_2 .

Fluorescence Microscopy Experiments. Raw 264.7 cells were seeded in a 96-well cell culture plate at a density of 5×10^3 cells per well and were allowed to attach for 24 h. Paraquat **G1**, **WP6**, and the host–guest complex **WP6** were added at different concentrations (from 30 to 500 μM). After 24 h, the medium was removed and washed with PBS. Then cells were stained with fluorescein diacetate (5 $\mu\text{g}/\text{mL}$) for 5 min in cell culture medium. The cells were washed and then visualized under a fluorescence microscope (Olympus IX81).

Evaluation of Cytotoxicity. The cytotoxicity of paraquat **G1**, **WP6**, and host–guest complex **WP6** against Raw 264.7 cells were determined by 3-(4,5-dimethylthiazol-2-yl)-2,5-diphenyl tetrazolium bromide (MTT) assay in a 96-well cell culture plate. All solutions were sterilized by filtration with a 0.22 μm filter before tests. Raw 264.7 cells were seeded at a density of 1×10^4 cells/well in a 96-well plate, and incubated for 24 h for attachment. Cells were then incubated with fresh serum-supplemented DMEM without/with paraquat, **WP6**, and the host–guest complex **WP6** at various concentrations for 24 h. Then, 20 μL of MTT solution (5 mg/mL) was added to each well. After 4 h of incubation at 37 °C, the MTT solution was removed, and the insoluble formazan crystals that formed were dissolved in 100 μL of dimethylsulfoxide (DMSO). The absorbance of the formazan product was measured at 570 nm using a spectrophotometer (Bio-Rad Model 680). Untreated cells in media were used as a control. All experiments were carried out with three replicates.

Statistical Analysis. Data are expressed as mean standard deviation (SD). Analysis of variance (ANOVA), followed by Student's *t*-test, was used to determine the significant differences among the groups, and *p*-values less than 0.05 were considered significantly.

3. RESULTS AND DISCUSSION

Host–Guest Complexation Studies. The water-soluble pillar[6]arene **WP6** was prepared according to a method previously reported by us.^{8g} Paraquat **G1** ($\text{PQ}^{2+} \cdot 2\text{Br}^-$) is

commercially available. The complexation of WP6 with G1 was first studied by ^1H NMR spectroscopy. As shown in Figure 1c,

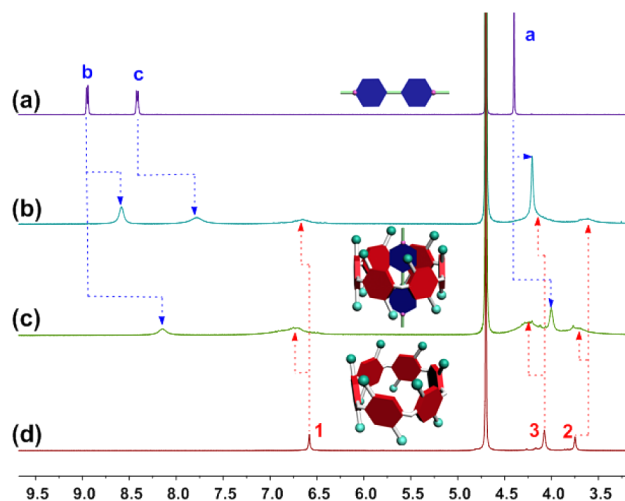


Figure 1. ^1H NMR spectra (500 MHz, D_2O , room temperature): (a) G1 (1.00 mM); (b) G1 (3.00 mM) and WP6 (1.00 mM); (c) G1 (1.00 mM) and WP6 (1.00 mM); (d) WP6 (1.00 mM).

when 1 equiv of WP6 was added into a D_2O solution of G1 (1.00 mM), the signals related to the protons on G1 shifted upfield significantly. Additionally, extensive broadening effect occurred when G1 interacted with WP6 due to complexation dynamics.^{8d} The resonance peak related to protons H_c disappeared after complexation caused by broadening effect. The reason is that these protons located within the cavity of WP6 and were shielded by the electron-rich cyclic structure upon forming a threaded structure between WP6 and G1. In order to further study the chemical shift changes of the protons corresponding to the host and the guest, excess G1 (3 equiv) was added. Broadening effect could also be observed, while the signals related to the protons of WP6 and G1 appeared clearly (spectrum b in Figure 1). Protons H_b and H_c on the 4,4'-bipyridinium unit shifted upfield dramatically ($\Delta\delta = -0.38$ and -0.64 ppm, respectively), which resulted from the formation of a threaded structure between WP6 and G1. The peak for protons H_a shifted upfield from 4.40 to 4.21 ppm. Actually, the chemical shift changes of protons H_b and H_c were larger than that of H_a ,^{7m} which was in good agreement with the crystal structure between *per*-hydroxylated pillar[6]arene and paraquat.^{8e} On the other hand, the protons on WP6 also exhibited slight chemical shift changes due to the interactions between WP6 and G1. 2D NOESY is a useful tool to study the relative positions of building components in host–guest inclusion complexes. From the 2D NOESY spectrum of a solution of 10.0 mM WP6 and 30.0 mM G1 (Figure S9), correlations were observed between protons H_b of the axle G1 and protons H_1 on WP6, suggesting that G1 was threaded into the cavity of WP6. Therefore, from these proton NMR and NOESY investigations, we can draw a conclusion that when G1 penetrated into the cavity of WP6, a 1:1 [2]pseudorotaxane WP6⊃G1 formed. In this pseudorotaxane, protons H_b and H_c located in the electron-rich cavity of WP6, while protons H_a were outside of the cavity.

For the estimation of the association constant for the complexation between WP6 and G1, fluorescence titrations of WP6 with G1 were conducted at room temperature in water.

As shown in Figure 2a, the quenching of fluorescence intensity was found to be significant upon gradual addition of G1. A

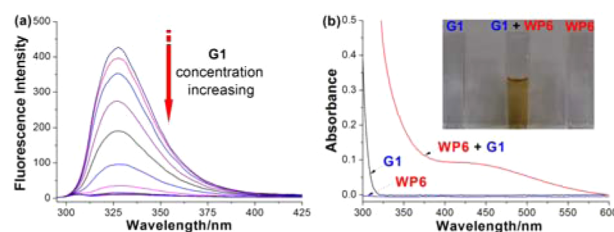


Figure 2. (a) Fluorescence spectra of WP6 (2.00×10^{-6} M) in aqueous solution at room temperature with different concentrations of G1: 0, 0.249, 0.739, 1.46, 2.38, 3.49, 4.55, 6.52, 8.33, 10.0, 11.5, and 12.9×10^{-6} M^{-1} . (b) UV–vis spectra of G1, WP6, and G1 in the presence of 1 equiv of WP6 (2.50×10^{-4} M) in water. The inserted photo shows the solution color change upon the complexation of WP6 with 1 equiv of G1.

mole ratio plot based on the fluorescence titration experiments demonstrated that the complex between WP6 and G1 had a 1:1 stoichiometry (Figure S7). Additionally, the association constant (K_a) was calculated to be $(1.02 \pm 0.10) \times 10^8 \text{ M}^{-1}$ by using a nonlinear curve-fitting method (Figure S8), which is much higher than the corresponding K_a value, $(8.20 \pm 1.70) \times 10^4 \text{ M}^{-1}$,^{7c} for the complexation between the analogous water-soluble pillar[5]arene WP5 (Chart 1) and paraquat G1. The reason is that the width of 4,4'-bipyridinium group (6.3 Å, all sizes are calculated on the basis of van der Waals radii)^{6a} is larger than the internal cavity of pillar[5]arenes (~ 4.7 Å).^{8d} From the crystal structure of the complex between *per*-hydroxylated pillar[6]arene and paraquat reported by our group,^{8e} we know that the size of 4,4'-bipyridinium unit is suitable for the internal cavity of pillar[6]arenes (~ 6.7 Å).^{8d} This match in size between pillar[6]arenes and paraquat resulted in the more efficient interactions between WP6 and G1 (Figure S3). We speculated that the formation of the complex between WP6 and paraquat was mainly driven by multiple electrostatic interactions between the carboxylate anionic groups on the rigid pillar[6]arene receptor platform and the cationic 4,4'-bipyridinium unit of the paraquat guest, hydrophobic interactions, and π – π stacking interactions between the benzene rings on the pillar[6]arene host and the pyridinium rings on the paraquat guest in aqueous solution. The extremely high binding affinity of this host–guest system should be attributed to the cooperativity of these noncovalent interactions.

Further evidence for the formation of a stable host–guest complex WP6⊃G1 was obtained from UV–vis absorption spectroscopy. When WP6 and G1 (molar ratio = 1:1) were mixed in water, the resulting solution had a yellow color, indicating the formation of a typical charge-transfer complex (Figure 2b).¹⁰ The spectrum of an equimolar aqueous solution of WP6 and G1 exhibits a broad absorption above 400 nm which corresponds to the characteristic absorption of the charge-transfer complex between electron-rich WP6 and electron-deficient G1. On the other hand, a notable red-shift was observed (Figure 2b and Figure S4), showing electronic communication between WP6 and G1.^{8g}

pH-Responsiveness. The molecular recognition of WP6 to G1 in water not only has high binding strength but also pH-responsiveness. ^1H NMR (Figure S10) and UV–vis spectroscopy (Figure S11) provided convincing evidence for the pH-

responsive complexation between **WP6** and **G1**. When the solution pH was adjusted to 6.0, the carboxylic groups on both rims of the pillar[6]arene were protonated to insoluble carboxylic acid groups. The water-soluble host precipitated from the solution, resulting in the disappearance of the signals related to the protons on the host (Figure S10b). For the water-soluble guest **G1**, it dethreaded from the cavity of **WP6** and kept staying in D_2O when the host changed into insoluble precipitation, so only the resonances associated with **G1** existed in the 1H NMR spectrum. On the other hand, the insoluble $-COOH$ units were deprotonated and **WP6** was soluble in water again when the pH of the solution recovered to 7.4. The peaks related to the protons on **G1** shifted upfield and exhibited remarkable complexation-induced broadening effects again (Figure S10c), indicating the reformation of **WP6** \supset **G1**. The pH-responsiveness of **WP6** \supset **G1** was also confirmed using UV-vis spectroscopy. As shown in Figure S11, when the pH of the solution containing equivalent amount of **WP6** and **G1** changed from 7.4 to 6.0, the characteristic absorption corresponding to the charge-transfer complex between **WP6** and **G1** disappeared, which indicated that the interactions between **WP6** and **G1** were damaged and **G1** migrated outside of the cavity. On the contrary, the characteristic absorption of the charge-transfer complex appeared again when the solution pH increased to 7.4 because **G1** rethreaded into the cavity of **WP6** (Figure S11c). These results demonstrated that the threading and dethreading processes of [2]pseudorotaxane **WP6** \supset **G1** could be reversibly controlled by adjusting the solution pH.

Controllable Self-Assembly. After the establishment of the new pillar[6]arene/paraquat recognition motif in water, we further applied it to construct a supra-amphiphile¹¹ and utilize it in controllable self-assembly. **G2** itself is an amphiphilic molecule that contains a long alkyl chain as hydrophobic part and 4,4'-bipyridinium unit as hydrophilic part. The aggregation behavior of **G2** was first studied by fluorescence spectra of the solutions containing pyrene probe molecules ($1.00 \mu M$). The quenching of fluorescence observed in the emission spectrum of **G2** was not notable (Figure 3). On the contrary, the relative fluorescence intensity of pyrene diminishes dramatically upon addition of **G2** in the presence of **WP6** ($2.00 \times 10^{-5} M$)

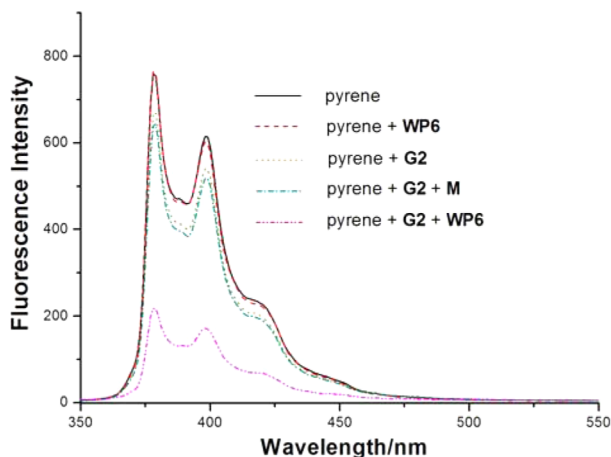


Figure 3. Fluorescence emission spectra of pyrene in aqueous solutions of **WP6**, **G2**, **G2 + M**, and **G2 + WP6** at room temperature. [**WP6**] = 0.0400 mM , [**G2**] = 0.0800 mM , [**M**] = 0.200 mM , and [pyrene] = $1.00 \mu M$.

(Figure S12). The efficient quenching can be explained by the proximity of the pyrene molecules to the viologen headgroup caused by charge-transfer interaction between electron-rich pyrene and electron-deficient 4,4'-bipyridinium unit. This phenomenon was consistent with the increasingly widespread view that nonpolar molecules like pyrene are solubilized near the Stern layer in ionic micelles,¹² which also proves the formation of amphiphilic aggregation. It is noted that **WP6** has no tendency to self-aggregation in aqueous solution at this concentration. On the other hand, no notable quenching of fluorescence occurred when the model compound (**M**, Chart 1) was added to the solution of **G2** in the presence of pyrene probe molecules (Figure 3). These phenomena undoubtedly indicated that the host-guest complexation is the crucial factor leading to the aggregation of **G2**, where the electrostatic interactions, hydrophobic interactions, and π - π stacking interactions reinforce the complex stability.

From fluorescence experiments, we knew that **WP6** \supset **G2** could form nanostructural aggregates due to the host-guest interactions between **WP6** and **G2**. Therefore, it is necessary to determine the best molar fraction of **WP6** leading to aggregation. Figure S13a showed the absorbance evolution at 378 nm as a function of the **WP6** concentration with a fixed **G2** concentration at $8.00 \times 10^{-5} M$. Upon gradual addition of **WP6**, the fluorescent intensity underwent a sharp decrease when the concentration of **WP6** reached $4.00 \times 10^{-5} M$. Then, an inverse increase was observed upon further addition of **WP6**. The inflection appears when the **WP6**/**G2** molar ratio is 0.5 (Figure S13b). In the left-hand portion of inflection, **WP6** and **G2** form a higher-order complex with a tendency toward supra-amphiphilic aggregation, whereas in the right-hand portion of inflection, excess **WP6** in solution leads to the formation of a simple 1:1 inclusion complex rather than higher-order aggregation.^{3g}

The critical aggregation concentration (CAC) of **G2** was calculated to be about $(3.44 \pm 0.21) \times 10^{-4} M$ using concentration-dependent conductivity (Figure S15). Excitingly, the critical aggregation concentration of **G2** in the presence of **WP6** was decreased to be about $(1.95 \pm 0.13) \times 10^{-5} M$ (Figure 4b). The CAC value of **G2** decreases pronouncedly by a factor of ca. 17.6 due to the formation of a stable host-guest complex with **WP6**. As shown in Figure 4a, an equimolar solution of $5.00 \times 10^{-5} M$ **WP6** and **G2** in water exhibits a clear Tyndall effect, while for $5.00 \times 10^{-5} M$ **G2** in water, Tyndall effect could not be observed because it has higher CAC value. This phenomenon indicated that no aggregates formed at this concentration for **G2** itself. On the other hand, with much lower CAC value of **WP6** \supset **G2**, this host-guest system could form nanostructural aggregates. Certainly, Tyndall effect could be observed for both **G2** and **WP6** \supset **G2** when the concentration increased to $5.00 \times 10^{-4} M$ because this concentration was higher than both of the CAC values of **G2** and **WP6** \supset **G2**, indicating the formation of self-assembled aggregates for both **G2** and **WP6** \supset **G2** at this concentration (Figure 4c).

Transmission electron microscopy (TEM) experiments assisted in the visualization of the nanostructures of **G2** and **WP6** \supset **G2**. As shown in Figure 4d, solid spherical structures formed by **G2** alone with the average diameter about 7.0 nm were observed when the concentration was higher than its CAC value. The diameter is near to the length of two **G2** molecules, confirming the formation of micelles. Upon addition of **WP6**, a supra-amphiphile formed on the basis of the novel recognition

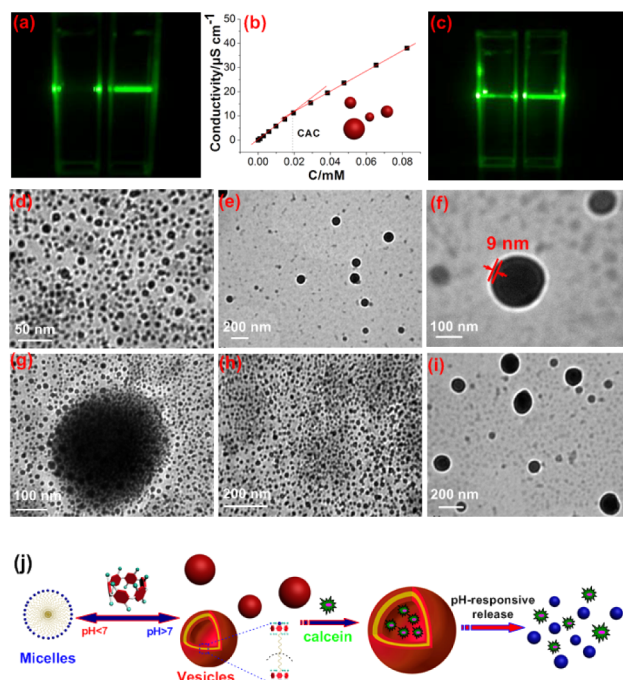


Figure 4. (a) Tyndall effect of free G2 (left) and WP6⊃G2 complex (right). $[G2] = [WP6] = 5.00 \times 10^{-5}$ M. (b) The concentration-dependent conductivity of G2 in the presence of WP6. The critical aggregation concentration (CAC) was determined to be $(1.95 \pm 0.13) \times 10^{-5}$ M for WP6⊃G2. (c) Tyndall effect of free G2 (left) and WP6⊃G2 complex (right). $[G2] = [WP6] = 5.00 \times 10^{-4}$ M. TEM images: (d) G2; (e) WP6⊃G2; (f) enlarged image of e (scale bar = 100 nm); (g) the intermediate state from vesicles to micelles (scale bar = 100 nm); (h) WP6⊃G2 when the pH of the solution is 6.0 (scale bar = 200 nm); (i) WP6⊃G2 when the pH of the solution is 7.4 (scale bar = 200 nm). (j) The illustration of the formation of the aggregates and the process of pH-responsive release of calcein molecules.

motif, resulting in the significant changes in the aggregation structures. Vesicles with an average diameter about 170 nm were observed (Figure 4e). The thickness of the hollow vesicles was calculated to be about 9 nm from TEM image (Figure 4f), suggesting that the vesicles have a bilayer wall. It should be noted that the extended length of the 1:1 [2]pseudorotaxane is about 3.0 nm. The fact is that the thickness of the vesicles is little larger than the extended length of two pseudorotaxanes due to the swollen effect.^{11f} From these data, we knew that the packing structure of the pseudorotaxanes in the membrane of the vesicles formed by G2 and WP6 was in an antiparallel packing pattern (Figure 4j).

The above demonstrated pH responsiveness of the complexation between WP6 and G1 was used to control the aggregation nanostructure from WP6⊃G2 by simply changing the solution pH. As shown in Figure 4h, micelles with the diameter about 7.0 nm reappeared by adjusting the solution pH to 6.0. Moreover, when the pH was slightly higher than 7.0, vesicles rather than micelles formed in solution again with the same thickness of the membrane shown in Figure 4f (Figure S16c), proving the pH-responsive self-assembly. Interestingly, the intermediate state from vesicles to micelles was revealed through TEM as shown in Figures 4g and S16a. When the pH was adjusted to 6.0, the vesicles were swelled and split into hundreds of micelles with similar diameter as shown in Figure 4d,h. The vesicles could be obtained again when the pH was adjusted to 7.4 (Figure 4i).

A mechanism was proposed to explain why the shape of G2 aggregates transforms from micelles to vesicles after its complexation with WP6 (Figure 4j). The microassembled structure of the aggregates formed by amphiphiles is determined by the curvature of the membrane.¹ⁱ When this amphiphilic guest is dissolved in water, the hydrophobic part tends to aggregate while the hydrophilic part favors to stay in water, generating micelles. Accompanied with the addition of WP6, the hydrophilic head of G2 containing the water-soluble 4,4'-bipyridinium unit threaded into the cavity of WP6 driven by electrostatic interactions, hydrophobic interactions, and π - π stacking interactions, forming a 1:1 [2]pseudorotaxane structural supra-amphiphile. The UV-vis spectrum exhibits a characteristic absorption of the charge-transfer complex between WP6 and G2 (Figure S5c), confirming the formation of WP6⊃G2. Due to the steric hindrance and the electrostatic repulsion generated upon insertion of the WP6 molecules, the formation of a vesicular structure with low curvature^{1i,8g} is obtained. When the solution pH was adjusted to 6.0, WP6 precipitated from the solution, resulting in the damage of the complexation between the hydrophilic head on G2 and WP6, so micelles rather than vesicles were observed. It should also be noted that a typical intermediate state from vesicles to micelles by adjusting the pH value of the solution to 6.0 (Figure 4g and Figure S16a) provided convincing evidence for the mechanism mentioned above. Therefore, self-assembly of this host-guest system can be reversibly controlled between micelles and vesicles by simply changing the solution pH.

The pH-responsive self-assembly of this host-guest system was further verified by dynamic light scattering (DLS) results. As shown in Figure 5a, the main diameter distribution of the

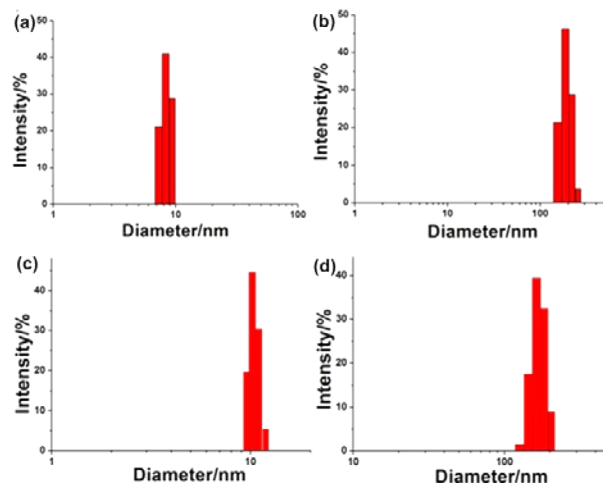


Figure 5. DLS results: (a) G2; (b) WP6⊃G2; (c) WP6⊃G2 when the pH of the solution is 6.0; (d) WP6⊃G2 when the pH of the solution is 7.4.

micelles formed from G2 alone is around 8.3 nm, which is in agreement with the corresponding TEM image shown in Figure 4d. Upon addition of WP6, the diameter of the aggregates formed by WP6⊃G2 increased to 185 nm (Figure 5b), also in accordance with the corresponding TEM image shown in Figure 4e. By adjusting the pH value of the solution to 6.0, the diameter of the aggregates returned back to 10.5 nm (Figure 5c), indicating the transformation from the vesicles to the micelles. On the other hand, by adjusting the pH value of the solution to 7.4, the diameter of the aggregates changed to about

203 nm due to the formation of the vesicles again (Figure 5d). These DLS experiments confirmed the reversible transformations between the vesicular structure and the micellar structure, providing convincing proof to support the pH-responsive self-assembly phenomena.

Controlled Release. The reversible transformations between micelles formed by **G2** alone and vesicles formed by the host–guest complex **WP6**⊃**G2** were then utilized for controlled release.¹³ The vesicles could encapsulate hydrophilic guest molecules within their interior at neutral or weakly basic condition and release the guest molecules in response to a decrease in pH. With this in mind, water-soluble calcein as a hydrophilic fluorescent guest was used to investigate the pH-responsive release. As shown in Figure S14, almost no fluorescence intensity could be observed corresponding to the characteristic absorbance of calcein, indicating that the calcein molecules stably located in the vesicles. By adjusting the pH of the solution to acidity, the release of calcein molecules from the inside of vesicles was achieved accompanied by an increase in fluorescence emission. This phenomenon can be explained by considering a pH-triggered vesicles–micelles transition. The decrease of pH resulted in the collapse of the vesicles into micelles with concomitant release of the encapsulated calcein molecules (Figure 4j).

Treatment of Paraquat Poisoning. Paraquat is showing an increasing number of scientific and technical applications not only as herbicides but also as probes to study DNA and zeolites, as components of electrochromic display devices, and as pro-oxidants in stress tests.¹⁴ However, its high toxicity poses considerable risks to human health, animals, and the environment.¹⁵ Absorption of paraquat into the digestive tract, respiratory tract, and skin may result in various diseases or even death. The main target organ for paraquat toxicity is the lung as a consequence of its accumulation, against a concentration gradient, through the highly developed polyamine uptake system, and due to its capacity to generate redox cycle.¹⁶ Several governmental organizations, including WHO, US EPA, and ECB et al. have therefore paid great attention to the use of paraquat because of its danger. Although many treatments have been proposed and attempted empirically on the basis of the pathologic mechanism of toxicity, none are supported by convincing clinical efficacy. The biochemical mechanism of PQ^{2+} toxicity was shown in Figure 6.¹⁷ The biochemical mechanism of PQ^{2+} toxicity involves the improve-

ment of intracellular levels of superoxide ($O_2^{\bullet-}$) by redox cycling. When PQ^{2+} enter the cells, it is enzymatically reduced to form the radical cation $PQ^{\bullet+}$, followed by the reduction of O_2 to $O_2^{\bullet-}$ by $PQ^{\bullet+}$ rapidly. The redox reaction between $PQ^{\bullet+}$ and O_2 is very fast, with a rate constant of $7.70 \times 10^8 \text{ M}^{-1} \text{ s}^{-1}$,¹⁸ resulting in the formation of other reactive oxygen species, such as H_2O_2 and HO^\bullet . H_2O_2 can further generate HO^\bullet through the Fenton reaction, which is the consequent toxic radical with deleterious cellular effects by oxidizing lipids, proteins, and nucleic acids.

With the toxic mechanism of paraquat in mind, we adopted a design utilizing this water-soluble pillar[6]arene to reduce the toxicity of paraquat **G1** to wrap up the toxic guest by forming a stable host–guest complex. The reasons were listed as follows: First, **G1** could be tightly included in the cavity of **WP6**, resulting in less opportunity for it to interact with the reducing agents in the cells. Second, as proved by cyclic voltammetry experiments (Figure S17), the reduction and oxidation processes of **G1** changed significantly upon complexation with **WP6**, which makes generation of their radical cations more difficult, resulting in the decrease of the toxic HO^\bullet .^{6f} This phenomenon can also be observed by the naked eye. The **G1** solution changed from colorless to yellow upon addition of **WP6** (Figure 2b), suggesting the formation of a stable charge-transfer complex between them as mentioned above. Third, **WP6** has the capability to bind transition metal ions due to the existence of six carboxylate anions on both sides of **WP6**, which could possibly restrain their catalytic effect. Therefore, the generation of HO^\bullet may be catalyzed by traces of transition metal ions. On the other hand, it is urgent to investigate the toxicity of **WP6** in order to further apply this macrocyclic host in biologically and pharmaceutically relevant fields since no studies about this have been reported up to now.

A simple evaluation of cytotoxicity for **G1**, **WP6**, and the host–guest complex **WP6**⊃**G1** at different concentrations against Raw 264.7 cells were carried out using a 3-(4,5-dimethylthiazol-2-yl)-2,5-diphenyl tetrazolium bromide (MTT) assay. Most compounds show low toxicity when they are in relatively low concentration, while for **WP6** the relative cell viability can reach about 50% in an extremely high concentration (500 μM), indicating very low toxicity of this water-soluble host (Figure 7). The toxicity of **WP6** is comparable or even lower than other host molecules which have been demonstrated with very low toxicity, such as cucurbit[*n*]uril.^{5c} These data provided convincing support that biologically and pharmaceutically relevant applications of **WP6** can be achieved in the future. On the other hand, the gradual addition of **G1** into the cells culture led to rapid decrease in relative cell viability. The shapes of the cells changed significantly, and the cell membrane was damaged seriously. These changes demonstrated that **G1** was toxic to the Raw 264.7 cells. In stark contrast, upon addition of the host–guest complex **WP6**⊃**G1**, the relative cell viability was higher than that of **G1** at the same concentration, which indicated that the toxicity of **G1** was significantly reduced upon formation of a stable host–guest complex. From Figure 7p, we knew that when the concentration was low (30 μM), the relative cell viabilities were all relatively high and the significant differences among these three groups were not so obvious. The reason was that, at this concentration, the contents of free **G1** in cells culture were quite low in both groups **G1** and **WP6**⊃**G1**. On the contrary, the relative cell viabilities were relatively low at high concentration (500 μM) caused by high content of free

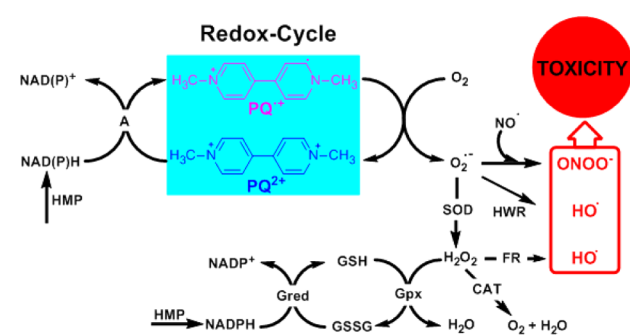


Figure 6. Schematic representation of the mechanism of paraquat toxicity.^{17b} A, cellular diaphorases; SOD, superoxide dismutase or spontaneously; CAT, catalase; GPx, glutathione peroxidase; Gred, glutathione reductase; $PQ^{\bullet+}$, paraquat cation radical; HMP, hexose monophosphate pathway; FR, Fenton reaction; HWR, Haber–Weiss reaction.

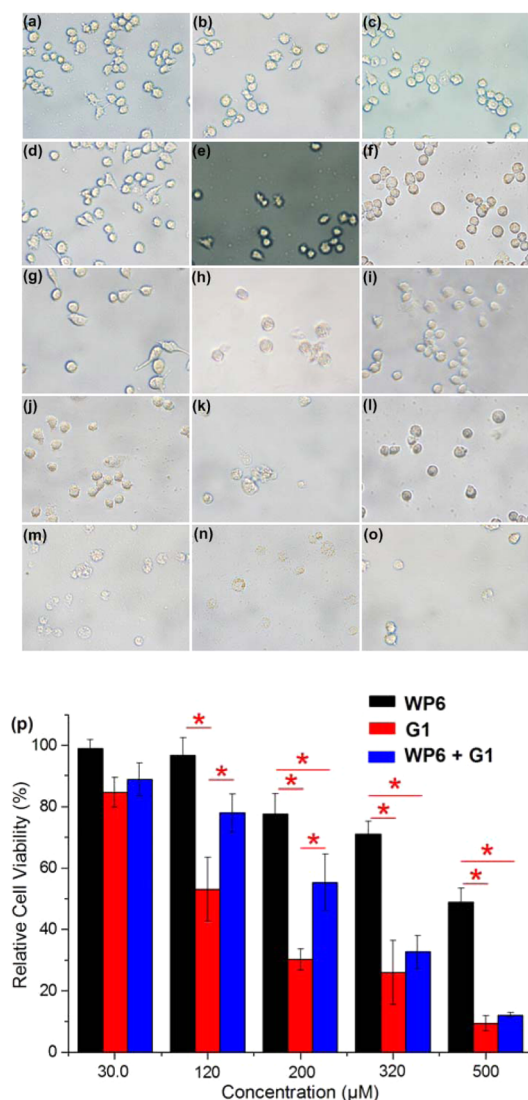


Figure 7. Fluorescence microscopy images of Raw 264.7 cells incubated with **G1**, **WP6**, and the host–guest complex **WP6⊃G1** under different conditions: (a) **WP6** (30 μM), (b) **G1** (30 μM), (c) **WP6⊃G1** (30 μM), (d) **WP6** (120 μM), (e) **G1** (120 μM), (f) **WP6⊃G1** (120 μM), (g) **WP6** (200 μM), (h) **G1** (200 μM), (i) **WP6⊃G1** (200 μM), (j) **WP6** (320 μM), (k) **G1** (320 μM), (l) **WP6⊃G1** (320 μM), (m) **WP6** (500 μM), (n) **G1** (500 μM), (o) **WP6⊃G1** (500 μM). (p) Cytotoxicity of **G1**, **WP6**, and the host–guest complex **WP6⊃G1** against Raw 264.7 cells. Statistically significant differences were observed ($p < 0.05$) (*).

G1 in cells culture. At middle concentration (for example, 200 μM), a part of the toxic **G1** molecules were wrapped up in the cavity of **WP6**. Therefore, the content of free **G1** in group **WP6⊃G1** was much lower, resulting in a higher relative cell viability than that of group **G1**. These results are in good agreement with our prediction mentioned above that **WP6** can be utilized to efficiently reduce the toxicity of paraquat.

CONCLUSIONS

In conclusion, a novel molecular recognition motif in water between **WP6** and paraquat was established. Due to the suitable size of pillar[6]arenes, paraquat could thread into the cavity of this water-soluble pillar[6]arene containing carboxylate anionic groups on both rims and form a stable 1:1 [2]pseudorotaxane-

type complex. On the basis of electrostatic interactions, hydrophobic interactions, and π - π stacking interactions, this host–guest complex has an extremely high association constant in water, about $(1.02 \pm 0.10) \times 10^8 \text{ M}^{-1}$. The threading and dethreading processes of this [2]pseudorotaxane could be reversibly controlled by changing the solution pH. Furthermore, we utilized this novel recognition motif in controllable self-assembly. Upon addition of **WP6**, micelles formed by **G2** alone changed into vesicles attributed to the formation of a stable host–guest complex with **WP6**. Due to the pH-responsiveness of **WP6**, the interactions between **G2** and **WP6** could be reversibly controlled by adjusting the pH, resulting in the reversible transformations between the micelles and vesicles. TEM experiments and DLS results provided convincing evidence for this controllable self-assembly. The controlled release of calcein was realized due to the pH-triggered vesicles–micelles transformation. Furthermore, a new approach to reduce the toxicity of paraquat efficiently based on the concept of host–guest chemistry was achieved, in which the toxicity of paraquat could be efficiently inhibited by the formation of a stable host–guest complex between **WP6** and paraquat. The present highly efficient recognition motif in aqueous media will find applications in the successful fabrication of large supramolecular systems, including supramolecular polymer¹⁹ and biologically/pharmaceutically fields.

ASSOCIATED CONTENT

Supporting Information

Experimental details and supporting data. This material is available free of charge via the Internet at <http://pubs.acs.org>.

AUTHOR INFORMATION

Corresponding Author

fhuang@zju.edu.cn

Notes

The authors declare no competing financial interest.

ACKNOWLEDGMENTS

This work was supported by the National Natural Science Foundation of China (20834004, 91027006, 21125417), the Fundamental Research Funds for the Central Universities (2012QNA3013), Program for New Century Excellent Talents in University, and Zhejiang Provincial Natural Science Foundation of China (R4100009). Thanks to Mr. Huan Zhou for his kindly assistance with electrochemical experiments.

REFERENCES

- (1) (a) Lehn, J.-M. *Supramolecular Chemistry*; VCH: Weinheim, 1995. (b) Sauvage, J.-P. *Acc. Chem. Res.* **1998**, *31*, 611–619. (c) Armaroli, N.; Balzani, V.; Collin, J.-P.; Gaviña, P.; Sauvage, J.-P.; Ventura, B. *J. Am. Chem. Soc.* **1999**, *121*, 4397–4480. (d) Collin, J.-P.; Dietrich-Buchecker, C.; Gaviña, P.; Jimene-Molero, M. C.; Sauvage, J.-P. *Acc. Chem. Res.* **2001**, *34*, 477–487. (e) Huang, F.; Fronczek, F. R.; Gibson, H. W. *J. Am. Chem. Soc.* **2003**, *125*, 9272–9273. (f) Huang, F.; Gibson, H. W. *J. Am. Chem. Soc.* **2004**, *126*, 14738–14739. (g) Jonkheijm, P.; Meijer, E. W. *Science* **2006**, *313*, 80–83. (h) Kay, E. R.; Leigh, D. A.; Zerbetto, F. *Angew. Chem., Int. Ed.* **2007**, *46*, 72–191. (i) Wang, C.; Yin, S.; Chen, S.; Xu, H.; Wang, Z.; Zhang, X. *Angew. Chem., Int. Ed.* **2008**, *47*, 9049–9052. (j) Wang, F.; Zhang, J.; Ding, X.; Dong, S.; Liu, M.; Zheng, B.; Li, S.; Wu, L.; Yu, Y.; Gibson, H. W.; Huang, F. *Angew. Chem., Int. Ed.* **2010**, *49*, 1090–1094. (k) Yan, X.; Wang, F.; Zheng, B.; Huang, F. *Chem. Soc. Rev.* **2012**, *41*, 6042–6065.

- (2) (a) Davidson, G. J. E.; Loeb, S. J. *Angew. Chem., Int. Ed.* **2003**, *42*, 74–77. (b) Huang, F.; Nagvekar, D. S.; Slobodnick, C.; Gibson, H. W. *J. Am. Chem. Soc.* **2005**, *127*, 484–485. (c) Huang, F.; Lam, M.; Mahan, E. J.; Rheingold, A. L.; Gibson, H. W. *Chem. Commun.* **2005**, 3268–3270. (d) Liu, Y.; Bruneau, A.; He, J.; Abliz, Z. *Org. Lett.* **2008**, *10*, 765–768. (e) Niu, Z.; Gibson, H. W. *Chem. Rev.* **2009**, *109*, 6024–6046. (f) Davidson, G. J. E.; Sharma, S.; Loeb, S. J. *Angew. Chem., Int. Ed.* **2010**, *49*, 4938–4942. (g) Jiang, W.; Schäfer, A.; Mohr, P. C.; Schalley, C. A. *J. Am. Chem. Soc.* **2010**, *132*, 2309–2320. (h) Niu, Z.; Huang, F.; Gibson, H. W. *J. Am. Chem. Soc.* **2011**, *133*, 2836–2839. (i) Zhu, K.; Vukotic, V. N.; Loeb, S. J. *Angew. Chem., Int. Ed.* **2012**, *51*, 2168–2172. (j) Qi, Z.; Molina, P. M.; Jiang, W.; Wang, Q.; Nowosinski, K.; Schulz, A.; Gradzielski, M.; Schalley, C. A. *Chem. Sci.* **2012**, *3*, 2073–2082. (k) Zheng, B.; Wang, F.; Dong, S.; Huang, F. *Chem. Soc. Rev.* **2012**, *41*, 1621–1636.
- (3) (a) Mirzozian, A.; Kaifer, A. E. *Chem. Commun.* **1999**, 1603–1604. (b) Harada, A. *Acc. Chem. Res.* **2001**, *34*, 456–464. (c) Terao, J.; Tang, A.; Michels, J. J.; Krivokapic, A.; Anderson, H. L. *Chem. Commun.* **2004**, 56–57. (d) Wang, Q.-C.; Qu, D.-H.; Ren, J.; Chen, K.; Tian, H. *Angew. Chem., Int. Ed.* **2004**, *43*, 2661–2665. (e) Tomatsu, I.; Hashidzume, A.; Harada, A. *J. Am. Chem. Soc.* **2006**, *128*, 2226–2227. (f) Liao, X.; Chen, G.; Liu, X.; Chen, W.; Chen, F.; Jiang, M. *Angew. Chem., Int. Ed.* **2010**, *49*, 4409–4413. (g) Wang, K.; Guo, D.-S.; Wang, X.; Liu, Y. *ACS Nano* **2011**, *5*, 2880–2894.
- (4) (a) Philip, I. E.; Kaifer, A. E. *J. Am. Chem. Soc.* **2002**, *124*, 12678–12679. (b) Guo, D.-S.; Liu, Y. *Chem. Soc. Rev.* **2012**, *41*, 5907–5921. (c) Guo, D.-S.; Wang, K.; Wang, Y.-X.; Liu, Y. *J. Am. Chem. Soc.* **2012**, *134*, 10244–10250.
- (5) (a) Gómez-Kaifer, W.; Ong, M.; Kaifer, A. E. *Org. Lett.* **2002**, *4*, 1791–1794. (b) Jeon, Y. J.; Kim, H.; Jon, S.; Selvapalam, N.; Seo, D. H.; Oh, I.; Park, C.-S.; Jung, S. R.; Koh, D.-S.; Kim, K. *J. Am. Chem. Soc.* **2004**, *126*, 15944–15945. (c) Uzunova, V. D.; Cullinane, C.; Brix, K.; Nau, W. M.; Day, A. I. *Org. Biomol. Chem.* **2010**, *8*, 2037–2042. (d) Lan, Y.; Loh, X. J.; Geng, J.; Walsh, Z.; Scherman, O. A. *Chem. Commun.* **2012**, 48, 8757–8759. (e) Loh, X. J.; Barrio, J.; Toh, P. P. C.; Lee, T.-C.; Jiao, D.; Rauwald, U.; Appel, E. A.; Scherman, O. A. *Biomacromolecules* **2012**, *13*, 84–91.
- (6) (a) Huang, F.; Gibson, H. W.; Bryant, W. S.; Nagvekar, D. S.; Fronczek, F. R. *J. Am. Chem. Soc.* **2003**, *125*, 9367–9371. (b) Huang, F.; Zakharov, L. N.; Rheingold, A. L.; Ashraf-Khorassani, M.; Gibson, H. W. *J. Org. Chem.* **2005**, *70*, 809–813. (c) Huang, F.; Switek, K. A.; Zakharov, L. N.; Fronczek, F. R.; Slobodnick, C.; Lam, M.; Golen, J. A.; Bryant, W. S.; Mason, P. E.; Rheingold, A. L.; Ashraf-Khorassani, M.; Gibson, H. W. *J. Org. Chem.* **2005**, *70*, 3231–3241. (d) Zong, Q.-S.; Chen, C.-F. *Org. Lett.* **2006**, *8*, 211–214. (e) Han, T.; Chen, C.-F. *Org. Lett.* **2006**, *8*, 1069–1072. (f) Wang, K.; Guo, D.-S.; Zhang, H.-Q.; Li, D.; Zheng, X.-L.; Liu, Y. *J. Med. Chem.* **2009**, *52*, 6402–6412. (g) Niu, Z.; Slobodnick, C.; Bonrad, K.; Huang, F.; Gibson, H. W. *Org. Lett.* **2011**, *13*, 2872–2875. (h) Guo, J.-B.; Han, Y.; Cao, J.; Chen, C.-F. *Org. Lett.* **2011**, *13*, 5688–5691. (i) Zhang, M.; Li, S.; Dong, S.; Chen, J.; Zheng, B.; Huang, F. *Macromolecules* **2011**, *44*, 9629–9643. (j) Zhang, M.; Zheng, B.; Huang, F. *Chem. Commun.* **2011**, 47, 10103–10105. (k) Li, C.; Xu, Q.; Li, J.; Yao, F.; Jia, X. *Org. Biomol. Chem.* **2010**, *8*, 1568–1576.
- (7) (a) Ogoshi, T.; Kanai, S.; Fujinami, S.; Yamagishi, T. A.; Nakamoto, Y. *J. Am. Chem. Soc.* **2008**, *130*, 5022–5023. (b) Zhang, Z.; Xia, B.; Han, C.; Yu, Y.; Huang, F. *Org. Lett.* **2010**, *12*, 2385–2387. (c) Ogoshi, T.; Hashizume, M.; Yamagishi, T.; Nakamoto, Y. *Chem. Commun.* **2010**, 46, 3708–3710. (d) Li, C.; Zhao, L.; Li, J.; Ding, X.; Chen, S.; Zhang, Q.; Yu, Y.; Jia, X. *Chem. Commun.* **2010**, 46, 9016–9018. (e) Zhang, Z.; Yu, G.; Han, C.; Liu, J.; Ding, X.; Yu, Y.; Huang, F. *Org. Lett.* **2011**, *13*, 4818–4821. (f) Zhang, Z.; Luo, Y.; Chen, J.; Dong, S.; Yu, Y.; Ma, Z.; Huang, F. *Angew. Chem., Int. Ed.* **2011**, *50*, 1397–1401. (g) Zhang, Z.; Luo, Y.; Xia, B.; Han, C.; Yu, Y.; Chen, X.; Huang, F. *Chem. Commun.* **2011**, 47, 2417–2419. (h) Strutt, N. L.; Forgan, R. S.; Spruell, J. M.; Botros, Y. Y.; Stoddart, J. F. *J. Am. Chem. Soc.* **2011**, *133*, 5668–5671. (i) Hu, X.-B.; Chen, L.; Si, W.; Yu, Y.; Hou, J.-L. *Chem. Commun.* **2011**, 47, 4694–4696. (j) Li, C.; Shu, X.; Li, J.; Chen, S.; Han, K.; Xu, M.; Hu, B.; Yu, Y.; Jia, X. *J. Org. Chem.* **2011**, *76*, 8458–8465. (k) Ma, Y.; Ji, X.; Xiang, F.; Chi, X.; Han, C.; He, J.; Abliz, Z.; Chen, W.; Huang, F. *Chem. Commun.* **2011**, 47, 12340–12342. (l) Yu, G.; Zhang, Z.; Han, C.; Xue, M.; Zhou, Q.; Huang, F. *Chem. Commun.* **2012**, 48, 2958–2960. (m) Zhang, Z.; Han, C.; Yu, G.; Huang, F. *Chem. Sci.* **2012**, *3*, 3026–3031. (n) Guan, Y.; Ni, M.; Hu, X.; Xiao, T.; Xiong, S.; Lin, C.; Wang, L. *Chem. Commun.* **2012**, 48, 8529–8531. (o) Duan, Q.; Xia, W.; Hu, X.; Ni, M.; Jiang, J.; Lin, C.; Pan, Y.; Wang, L. *Chem. Commun.* **2012**, 48, 8532–8534. (p) Hu, X.-B.; Chen, Z.; Tang, G.; Hou, J.-L.; Li, Z.-T. *J. Am. Chem. Soc.* **2012**, *134*, 8384–8387. (q) Han, C.; Yu, G.; Zhang, Z.; Huang, F. *Org. Lett.* **2012**, *14*, 1712–1715. (r) Yao, Y.; Xue, M.; Chen, J.; Zhang, M.; Huang, F. *J. Am. Chem. Soc.* **2012**, *134*, 15712–15715.
- (8) (a) Cao, D.; Kou, Y.; Liang, J.; Chen, Z.; Wang, L.; Meier, H. *Angew. Chem., Int. Ed.* **2009**, *48*, 9721–9723. (b) Han, C.; Ma, F.; Zhang, Z.; Xia, B.; Yu, Y.; Huang, F. *Org. Lett.* **2010**, *12*, 4360–4363. (c) Ma, Y.; Zhang, Z.; Ji, X.; Han, C.; He, J.; Abliz, Z.; Chen, W.; Huang, F. *Eur. J. Org. Chem.* **2011**, 27, 5331–5335. (d) Yu, G.; Han, C.; Zhang, Z.; Chen, J.; Yan, X.; Zheng, B.; Liu, S.; Huang, F. *J. Am. Chem. Soc.* **2012**, *134*, 8711–8717. (e) Ma, Y.; Chi, X.; Yan, X.; Liu, J.; Yao, Y.; Chen, W.; Huang, F.; Hou, J.-L. *Org. Lett.* **2012**, *14*, 1532–1535. (f) Xue, M.; Yang, Y.; Chi, X.; Zhang, Z.; Huang, F. *Acc. Chem. Res.* **2012**, *45*, 1294–1308. (g) Yu, G.; Xue, M.; Zhang, Z.; Li, J.; Han, C.; Huang, F. *J. Am. Chem. Soc.* **2012**, *134*, 13248–13251. (h) Cragg, P. J.; Sharma, K. *Chem. Soc. Rev.* **2012**, *41*, 597–607. (i) Ogoshi, T.; Kayama, H.; Yamafuji, D.; Aoki, T.; Yamagishi, T. *Chem. Sci.* **2012**, *3*, 3221–3226. (j) Han, C.; Zhang, Z.; Chi, X.; Zhang, M.; Yu, G.; Huang, F. *Acta Chim. Sin.* **2012**, *70*, 1775–1778.
- (9) (a) Zhang, H.; Strutt, N. L.; Stoll, R. S.; Li, H.; Zhu, Z.; Stoddart, J. F. *Chem. Commun.* **2011**, 47, 11420–11422. (b) Ogoshi, T.; Shiga, R.; Yamagishi, T. *J. Am. Chem. Soc.* **2012**, *134*, 4577–4580. (c) Strutt, N. L.; Iehl, D. F.-J.; Lalonde, M. B.; Snurr, R. Q.; Farha, O. K.; Hupp, J. T.; Stoddart, J. F. *J. Am. Chem. Soc.* **2012**, *134*, 17436–17439. (d) Ogoshi, T. *J. Inclusion Phenom. Macrocyclic Chem.* **2012**, *72*, 247–262. (e) Ogoshi, T.; Yamafuji, D.; Aoki, T.; Yamagishi, T. *Chem. Commun.* **2012**, 48, 6842–6844. (f) Nierengarten, I.; Guerra, S.; Holler, M.; Nierengarten, J.-F.; Deschenaux, R. *Chem. Commun.* **2012**, 48, 8072–8074.
- (10) (a) Naka, K.; Chujo, Y. *Langmuir* **2003**, *19*, 5496–5501. (b) Shimazaki, Y.; Yamamoto, M. *Langmuir* **1997**, *13*, 1385–1387.
- (11) (a) Wang, C.; Chen, Q.; Xu, H.; Wang, Z.; Zhang, X. *Adv. Mater.* **2010**, *22*, 2553–2555. (b) Wang, C.; Wang, Z.; Zhang, X. *Small* **2011**, *7*, 1379–1383. (c) Liu, K.; Wang, C.; Li, Z.; Zhang, X. *Angew. Chem., Int. Ed.* **2011**, *50*, 4952–4956. (d) Zhang, X.; Wang, C. *Chem. Soc. Rev.* **2011**, *40*, 94–101. (e) Wang, C.; Wang, Z.; Zhang, X. *Acc. Chem. Res.* **2012**, *45*, 608–618. (f) Liu, K.; Yao, Y.; Wang, C.; Liu, Y.; Li, Z.; Zhang, X. *Chem. Eur. J.* **2012**, *18*, 8622–8628.
- (12) Menger, F. M. *Acc. Chem. Res.* **1979**, *12*, 111–117.
- (13) (a) Lee, M.; Lee, S.-J.; Jiang, L.-H. *J. Am. Chem. Soc.* **2004**, *126*, 12724–12725. (b) Niu, J.; Shi, F.; Liu, Z.; Wang, Z.; Zhang, X. *Langmuir* **2007**, *23*, 6377–6384.
- (14) (a) Brun, A. M.; Harriman, A. *J. Am. Chem. Soc.* **1991**, *113*, 8153–8159. (b) Migliaccio, E.; Giorgio, M.; Mele, S.; Pelicci, G.; Reboldi, P.; Pandolfi, P. P.; Lanfranccone, L.; Pelicci, P. G. *Nature* **1999**, *402*, 309–313. (c) Bird, C. L.; Kuhn, A. T. *Chem. Soc. Rev.* **2007**, *10*, 49–82. (d) Muffat, J.; Walker, D. W.; Benzer, S. *Proc. Natl. Acad. Sci. U.S.A.* **2008**, *105*, 7088–7093.
- (15) (a) Biismuth, C.; Hall, A. H. *Paraquat Poisoning: Mechanisms, Prevention, Treatment*; Dekker: New York, 1995. (b) Dinis-Oliveira, R. J.; Remião, F.; Carmo, H.; Duarte, J. A.; Navarro, A. S.; Bastos, M. L.; Carvalho, F. *Neurotoxicology* **2006**, *27*, 1110–1122.
- (16) (a) Dusinska, M.; Kovacicova, Z.; Vallova, B.; Collins, A. *Carcinogenesis* **1998**, *19*, 809–812. (b) Dinis-Oliveira, R. J.; Duarte, J. A.; Sánchez-Navarro, A.; Remião, F.; Bastos, M. L.; Carvalho, F. *Crit. Rev. Toxicol.* **2008**, *38*, 13–71.
- (17) (a) Calderbank, A. *Control Res.* **1968**, *8*, 129–235. (b) Dinis-Oliveira, R. J.; Sousa, C.; Remião, F.; Duarte, J. A.; Navarro, A. S.; Bastos, M. L.; Carvalho, F. *Free Radicals Biol. Med.* **2007**, *42*, 1017–1028. (c) Dinis-Oliveira, R. J.; Pontes, H.; Bastos, M. L.; Remião, F.; Duarte, J. A.; Carvalho, F. *Toxicology* **2009**, *255*, 187–193.

(18) Farrington, J. A.; Ebert, M.; Land, E. J.; Fletcher, K. *Biochim. Biophys. Acta* **1973**, *314*, 372–381.

(19) (a) Ligthart, G. B. W. L.; Ohkawa, H.; Sijbesma, R. P.; Meijer, E. *W. J. Am. Chem. Soc.* **2005**, *127*, 810–811. (b) Park, T.; Zimmerman, S. C.; Nakashima, S. *J. Am. Chem. Soc.* **2005**, *127*, 6520–6521. (c) Huang, F.; Nagvekar, D. S.; Zhou, X.; Gibson, H. W. *Macromolecules* **2007**, *40*, 3561–3567. (d) Rehm, T. H.; Schmuck, C. *Chem. Soc. Rev.* **2010**, *39*, 3597–3611. (e) Hu, X.-Y.; Zhang, P.; Wu, X.; Xia, W.; Xiao, T.; Jiang, J.; Lin, C.; Wang, L. *Polym. Chem.* **2012**, *3*, 3060–3063. (f) Hu, X.-Y.; Wu, X.; Duan, Q.; Xiao, T.; Lin, C.; Wang, L. *Org. Lett.* **2012**, *14*, 4826–4829.